ISSN 0965-5425, Computational Mathematics and Mathematical Physics, 2009, Vol. 49, No. 3, pp. 532–548. © Pleiades Publishing, Ltd., 2009.
Original Russian Text © T.G. Elizarova, E.V. Shil'nikov, 2009, published in Zhurnal Vychislitel'noi Matematiki i Matematicheskoi Fiziki, 2009, Vol. 49, No. 3, pp. 549–566.

Capabilities of a Quasi-Gasdynamic Algorithm as Applied to Inviscid Gas Flow Simulation

T. G. Elizarova and E. V. Shil'nikov

Institute for Mathematical Modeling, Russian Academy of Sciences, Miusskaya pl. 4a, Moscow, 125047 Russia
e-mail: telizar@mail.ru, shiva@imamod.ru

Received August 12, 2005;
in final form, September 16, 2008

Abstract—Ten well-known one-dimensional test problems reflecting the characteristic features of unsteady inviscid gas flows are successfully solved by a unified numerical algorithm based on the quasi-gasdynamic system of equations. In all the cases, the numerical solution converges to a self-similar one as the spatial grid is refined.

DOI: 10.1134/S0965542509030142

Keywords: quasi-gasdynamic algorithm, Euler equations, one-dimensional flows.

INTRODUCTION

The computation of unsteady compressible gas flows in the one-dimensional approximation is a visual tool for assessing the capabilities of numerical algorithms. At present, there are numerous examples of solutions to multidimensional problems that are used to compare numerical methods. However, the accuracy of the solution in such computations is generally determined not only by the numerical algorithm used but also by other factors, such as the structure of the spatial grid, the formulation of boundary conditions, and other circumstances that hamper the comparison of numerical algorithms. Additionally, a detailed theoretical analysis is available for one-dimensional inviscid gas flows, and self-similar solutions to Riemann problems for the Euler equations are known [1, 2], which serve as a reliable reference for verifying the accuracy and convergence of numerical solutions.

The tests discussed below can be found, for example, in [3, 4], where ten one-dimensional unsteady inviscid gas flows were computed by ten numerical algorithms that give a fairly complete picture of the capabilities of the finite-difference approach as applied to gas dynamics equations in Euler variables.

In this paper, the same tests are used to analyze the capabilities of a numerical algorithm based on the quasi-gasdynamic (QGD) equations (see, e.g., [5–7]). The QGD algorithm and related kinetically consistent difference schemes [8] have been successfully used for the numerical simulation of a wide class of viscous compressible gas flows. They were used to compute two- and three-dimensional unsteady flows, but one-dimensional problems received little attention. This paper fills this gap and demonstrates the applicability of the QGD algorithm to computations of nonstationary one-dimensional problems of various natures.

1. QUASI-GASDYNAMIC EQUATIONS AND THE NUMERICAL ALGORITHM

The quasi-gasdynamic equations for a one-dimensional plane flow in the conventional notation have the form

$$\frac{\partial \rho}{\partial t} + \frac{\partial j_m}{\partial x} = 0, \tag{1}$$

$$\frac{\partial \rho u}{\partial t} + \frac{\partial j_m u}{\partial x} + \frac{\partial p}{\partial x} = \frac{\partial \Pi}{\partial x}, \tag{2}$$

$$\frac{\partial E}{\partial t} + \frac{\partial j_m H}{\partial x} + \frac{\partial q}{\partial x} = \frac{\partial \Pi u}{\partial x}. \tag{3}$$

Table

Test	ρ_L	u_L	p_L	ρ_R	u_R	p_R	t_{fin}
1	1	0.75	1	0.125	0	0.1	0.2
2	1	–2	0.4	1	2	0.4	0.15
3	1	1	10^{-6}	1	–1	10^{-6}	1
3a	1	–19.59745	1000	1	–19.59745	0.01	0.012
4	5.99924	19.5975	460.894	5.99924	–6.19633	46.095	0.035
5	1.4	0	1	1	0	1	2
6	1.4	0.1	1	1	0.1	1	2
7	0.1261192	8.9047029	782.92899	6.591493	2.2654207	3.1544874	0.0039

Here, E and H are the total energy of a unit of volume and the total specific enthalpy, which are calculated by the formulas $E = \rho u^2/2 + p/(\gamma - 1)$ and $H = (E + p)/\rho$, respectively. The mass flux density is calculated as

$$j_m = \rho(u - w),$$

where

$$w = \frac{\tau}{\rho}\frac{\partial}{\partial x}(\rho u^2 + p).$$

The component of the viscous stress tensor involved in system (1)–(3) is defined as

$$\Pi = \frac{4}{3}\mu\frac{\partial u}{\partial x} + u\tau\left(\rho u\frac{\partial u}{\partial x} + \frac{\partial p}{\partial x}\right) + \tau\left(u\frac{\partial p}{\partial x} + \gamma p\frac{\partial u}{\partial x}\right).$$

The heat flux q is

$$q = -\kappa\frac{\partial T}{\partial x} - \tau\rho u\left[\frac{u}{\gamma - 1}\frac{\partial}{\partial x}\left(\frac{p}{\rho}\right) + pu\frac{\partial}{\partial x}\left(\frac{1}{\rho}\right)\right],$$

where $p = \rho RT$, μ is the dynamic viscosity, $\kappa = \mu\gamma R/[(\gamma - 1)\text{Pr}]$ is the thermal conductivity, γ is the adiabatic index, Pr is the Prandtl number, $\tau = \mu/(p\,\text{Sc})$ is a relaxation parameter having the dimension of time, and Sc is the Schmidt number.

For numerical convenience, system (1)–(3) is reduced in a dimensionless form by using the reference density ρ_0, the speed of sound $c_0 = \sqrt{\gamma RT_0}$, and the length L. The nondimensionalization procedure does not change the form of the equations.

We introduce a uniform grid in x with the mesh size h and a grid in time with the step Δt. All the flow parameters—the velocity, density, and pressure—are determined at grid nodes. The fluxes are determined at half-integer nodes. Problem (1)–(3) is approximated by a time explicit difference scheme of the form

$$\hat{\rho}_i = \rho_i - \frac{\Delta t}{h}(j_{m,\,i+1/2} - j_{m,\,i-1/2}), \tag{4}$$

$$\widehat{\rho_i u_i} = \rho_i u_i + \frac{\Delta t}{h}[(\Pi_{i+1/2} - \Pi_{i-1/2}) - (p_{i+1/2} - p_{i-1/2}) - (j_{m,\,i+1/2}u_{i+1/2} - j_{m,\,i-1/2}u_{i-1/2})], \tag{5}$$

$$\hat{E}_i = E_i + \frac{\Delta t}{h}\left[(\Pi_{i+1/2}u_{i+1/2} - \Pi_{i-1/2}u_{i-1/2}) - (q_{i+1/2} - q_{i-1/2})\right.$$
$$\left. - \left(\frac{j_{m,\,i+1/2}}{\rho_{i+1/2}}(E_{i+1/2} + p_{i+1/2}) - \frac{j_{m,\,i-1/2}}{\rho_{i-1/2}}(E_{i-1/2} + p_{i-1/2})\right)\right], \tag{6}$$

$$p_i = (\gamma - 1)\left(E_i - \frac{\rho_i u_i^2}{2}\right).$$

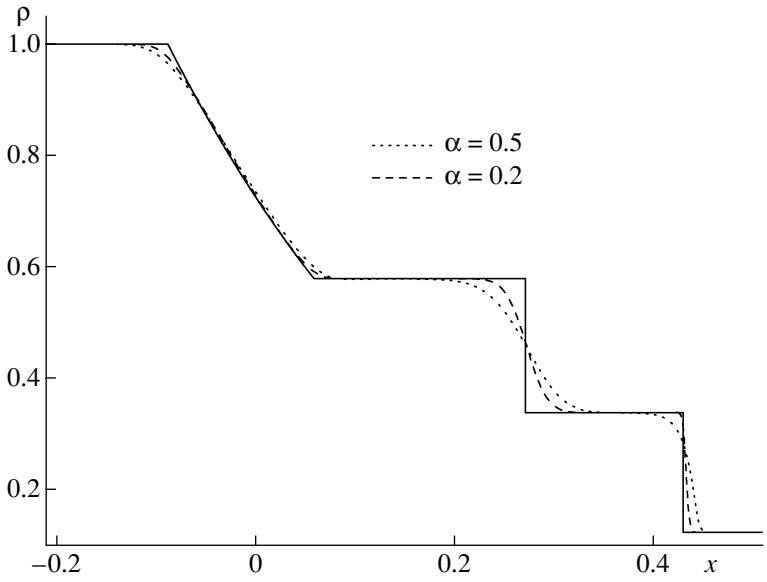

Fig. 1.

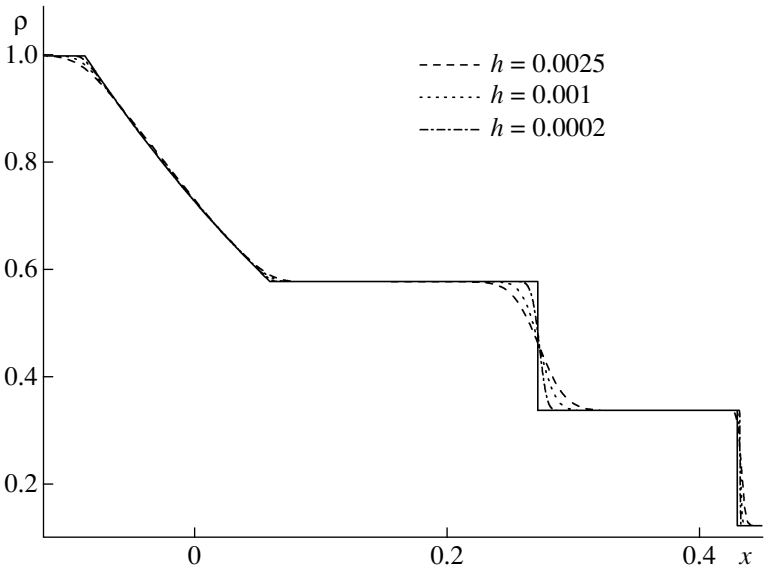

Fig. 2.

The discrete mass flux j_m has the form

$$j_{m,\,i+1/2} = \rho_{i+1/2}(u_{i+1/2} - w_{i+1/2}), \tag{7}$$

where the velocity addition is calculated as

$$w_{i+1/2} = \frac{\tau_{i+1/2}}{\rho_{i+1/2}}\frac{1}{h}(\rho_{i+1}u_{i+1}^2 + p_{i+1} - \rho_i u_i^2 - p_i). \tag{8}$$

The discrete expressions for Π and q are similar. The accuracy of difference scheme (4)–(8) is $O(h^2 + \Delta t)$.

When the Euler equations are solved numerically on the basis of system (1)–(3), all the dissipative terms (i.e., those with the coefficients μ, κ, and τ) are treated as artificial regularizers. The relaxation parameter,

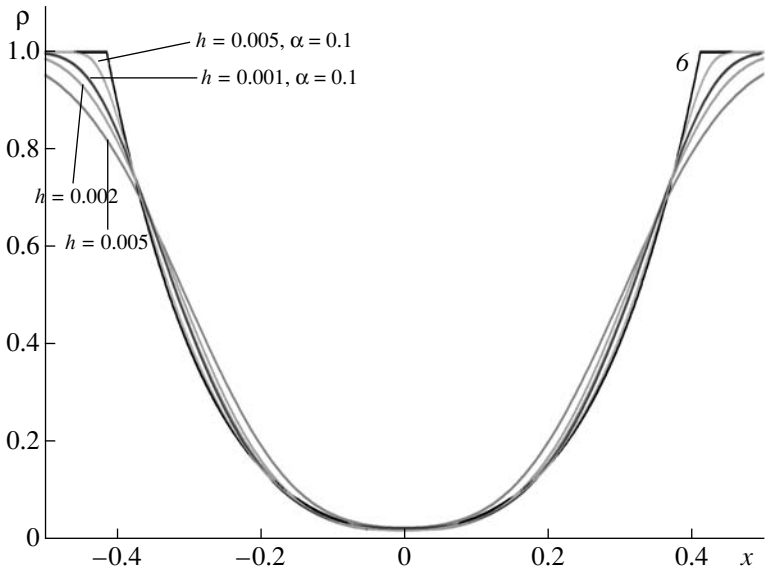

Fig. 3.

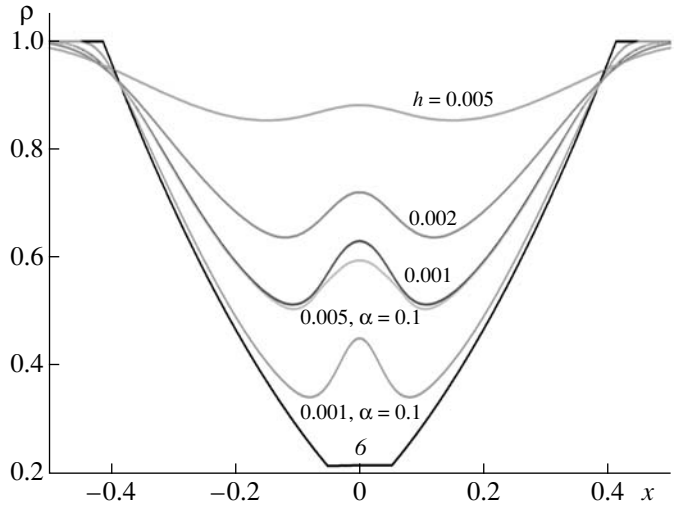

Fig. 4.

the viscosity, and the thermal conductivity coefficients are interrelated. In dimensionless form, they are calculated by the formulas

$$\tau = \alpha\frac{h}{c}, \quad \mu = \tau p\,\mathrm{Sc}, \quad \kappa = \frac{\tau p\,\mathrm{Sc}}{\mathrm{Pr}(\gamma-1)}, \tag{9}$$

where α is a numerical coefficient chosen, as a rule, in the range of 0.2–0.7. In most of the computations represented below, we set Pr = 1 and Sc = 1.

Formally, the order of scheme (4)–(9) is $O(\alpha h + \Delta t)$. The results reported below confirm that a decrease in α within a certain range is equivalent to a spatial mesh refined α times.

Difference scheme (4)–(9) satisfies the Courant stability condition. The time step is determined by the relation

$$\Delta t = \beta \min\left(\frac{h}{|u_i| + c_i}\right), \tag{10}$$

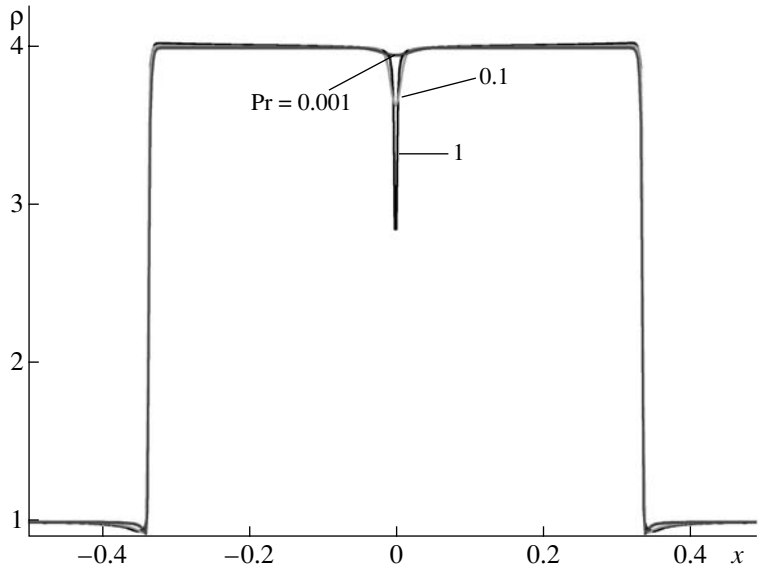

Fig. 5.

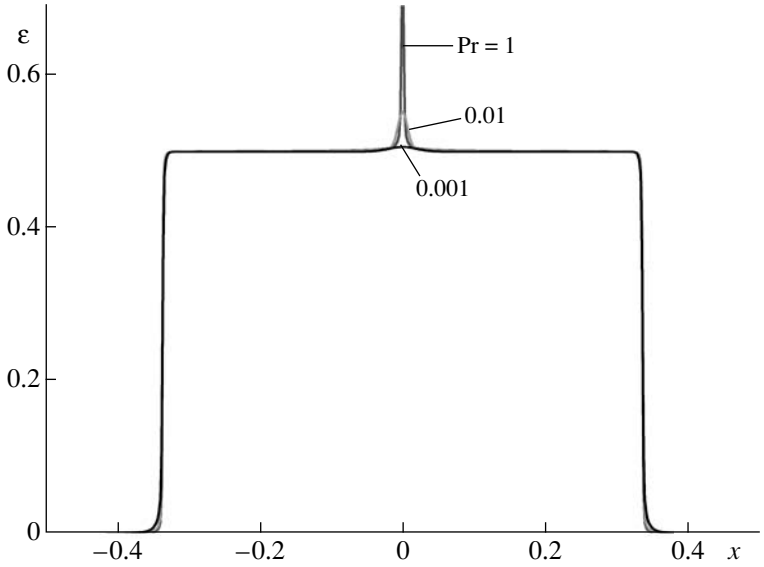

Fig. 6.

where β is a numerical coefficient ranging within 0.1–0.4 in most of the computations.

2. RIEMANN PROBLEMS

In this section, we consider the Riemann problems discussed in [3, 4]. They reflect the characteristic features of unsteady gas flows that are difficult for numerical simulation. The initial data for the Riemann problems are listed in the table with the notation used in [3, 4]. Specifically, the flow parameters on the left and right of the discontinuity are denoted by the indices L and R, respectively. The time at which the plots are constructed is given in the table and is denoted by t_{fin}.

The boundary conditions are the same as the corresponding initial conditions at the ends of the computational domain. In all the computations, $\gamma = 1.4$, except for Noh problem (3), in which $\gamma = 5/3$. The length of the computational domain is equal to 1. The discontinuity is at the point 0.

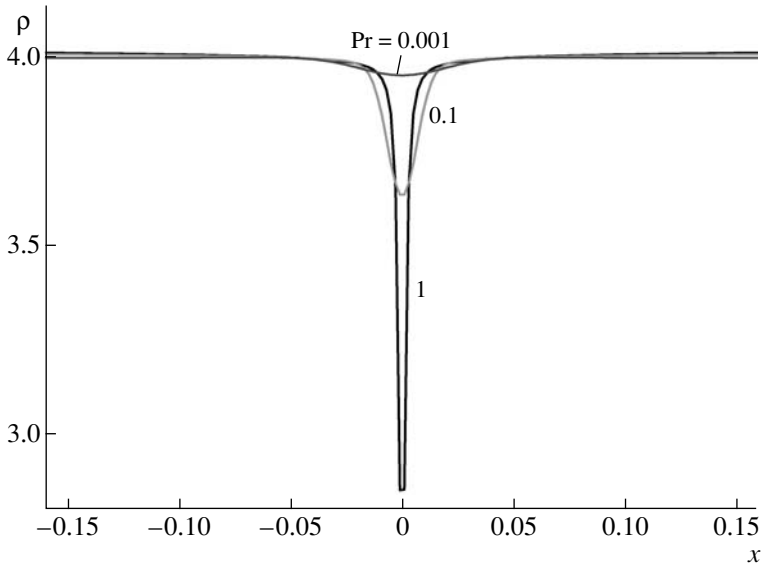

Fig. 7.

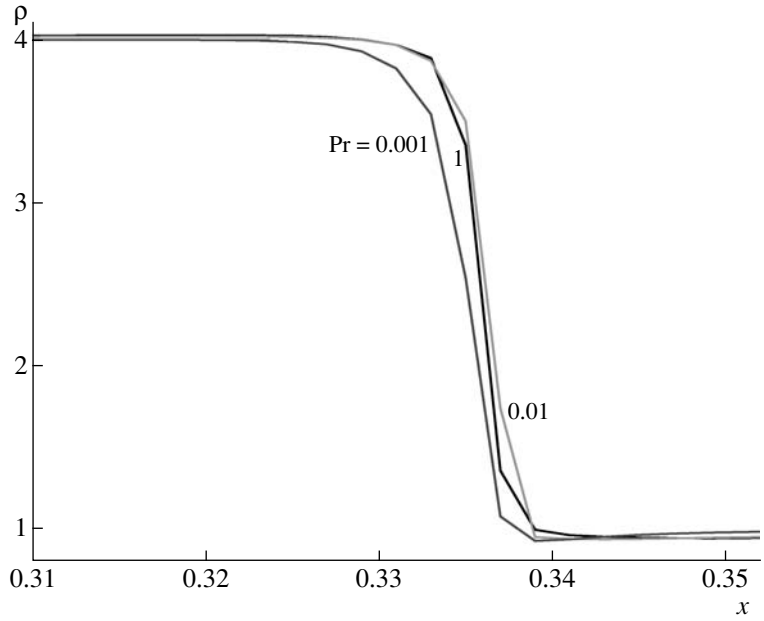

Fig. 8.

Problems 1, 2, and 4–6 were first suggested and numerically solved in [9]. In [10], problem 2 was solved using the QGD algorithm represented as a flux-splitting scheme. The Noh problem was first considered and numerically solved in [11].

Test 1. It is a version of the Sod problem. The resulting flow involves all the features characteristic of supersonic flows: sonic points at the boundaries of a rarefaction wave, a contact discontinuity, and a shock wave.

In the case of the QGD algorithm, this problem has a stable solution if $0.2 \le \alpha \le 0.5$ and $\beta = 0.4$ in formulas (9) and (10), respectively. A decrease in α in the computation of regularization parameter (9) leads to a more accurate numerical solution. Figure 1 shows the density distributions calculated on a spatial grid with the mesh size $h = 0.0025$. The solid line depicts the self-similar solution. Here and in the subsequent computations, the halved value of α is nearly equivalent to half a mesh size. However, the choice of $\alpha < 0.2$ leads

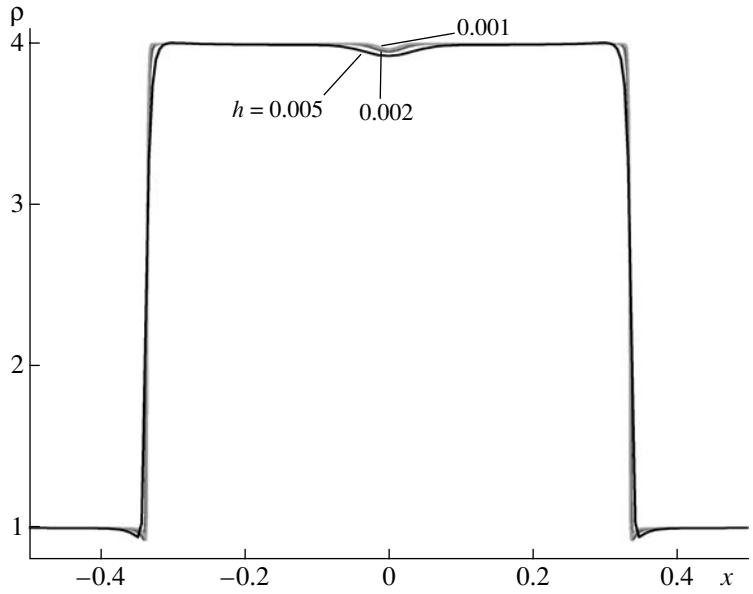

Fig. 9.

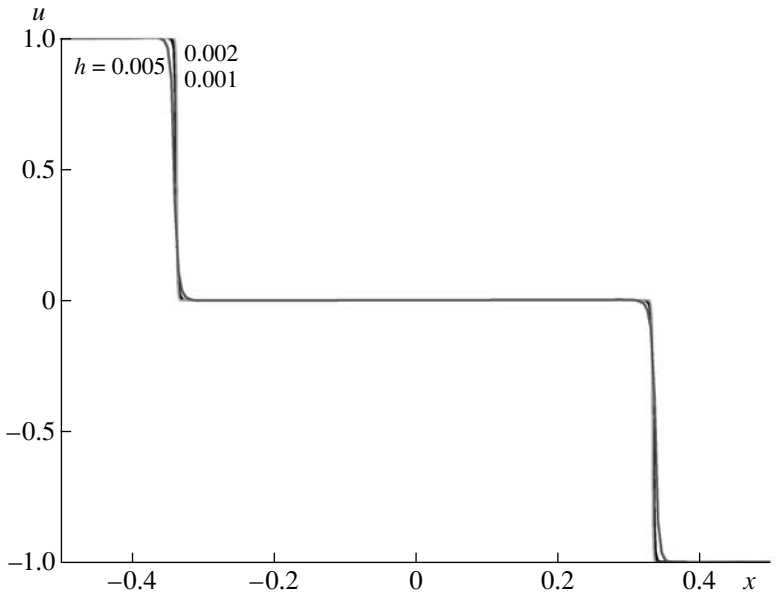

Fig. 10.

to computational instability, which can be eliminated by decreasing the time step, i.e., by decreasing β. Figure 2 demonstrates the convergence of the numerical solution at $\alpha = 0.2$ to the self-similar solution (solid line) as the spatial mesh size is decreased.

Test 2. The flow represents two rarefaction waves that propagate away from the center of the domain. The difficulty in the numerical solution of this problem is that the gas density and pressure at the center (between the diverging flows) are very low, while the internal energy $\varepsilon = p/[\rho(\gamma - 1)]$ does not tend to zero. It seems that there are no difference schemes in Eulerian variables that describe the behavior of the internal energy in this problem with high accuracy (see, e.g., [3, 4]).

In all the computations of this problem, we used $\beta = 0.1$. An increase in the time step led to numerical instability. Figures 3 and 4 show the gas density and internal energy as functions of the mesh size and α. Line *6* depicts the self-similar solution. Unless otherwise stated, $\alpha = 0.5$. A decrease in the regularization

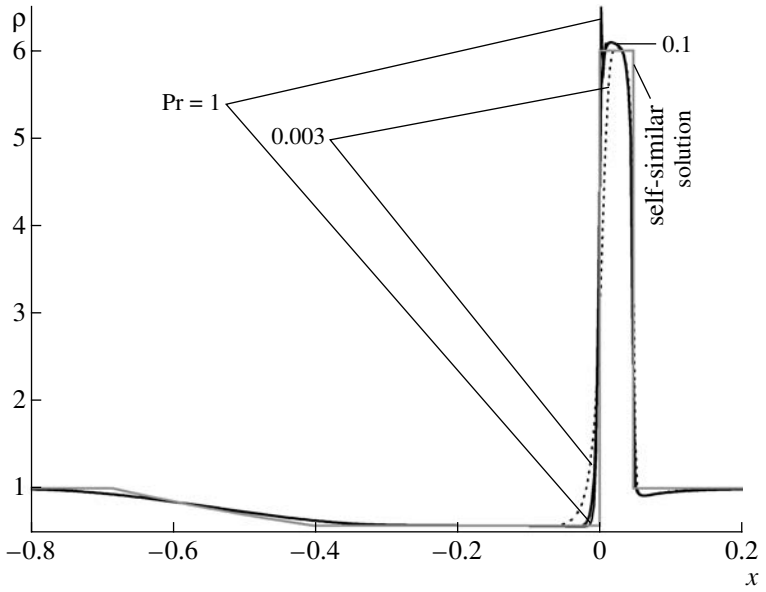

Fig. 11.

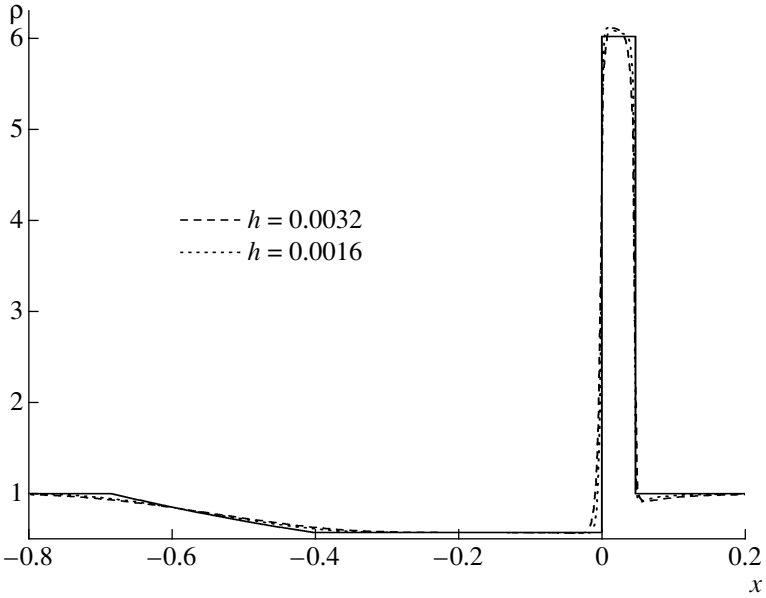

Fig. 12.

parameter or the mesh size leads to a more accurate numerical solution approaching the self-similar one. This can be seen most clearly in the plots of the internal energy (Fig. 4). The numerical results reveal that the velocity distribution converges rapidly as the mesh size is decreased.

Test 3. Noh problem. The flow is formed by the colliding of two hypersonic flows of a cold dense gas. As a result, two diverging "infinitely strong" shock waves are formed between which there remains a stationary gas with a constant density and pressure. Indeed, according to the initial conditions in the table, the speed of sound against the unperturbed background is $c = \sqrt{\gamma p_R/\rho_R} = 0.0013$. The velocity of the wave propagation is 1; i.e., the Mach number is $M = u_L/c = 775$. It is well known that the maximum Mach number reached in the terrestrial conditions is about ~30.

This problem was computed with $\alpha = 0.5$ and $\beta = 0.001$. At the first steps, a drop in the density and a rise in the temperature and internal energy (see Figs. 5–7, fragment) are observed at the center of the com-

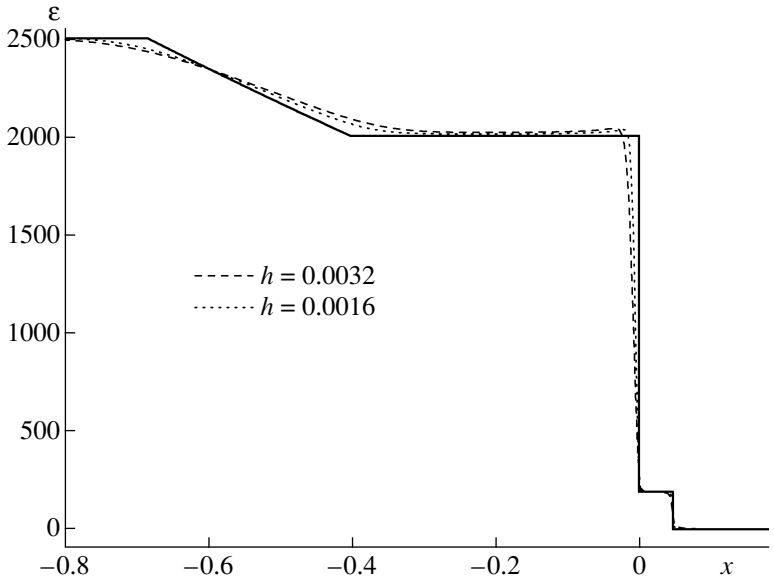

Fig. 13.

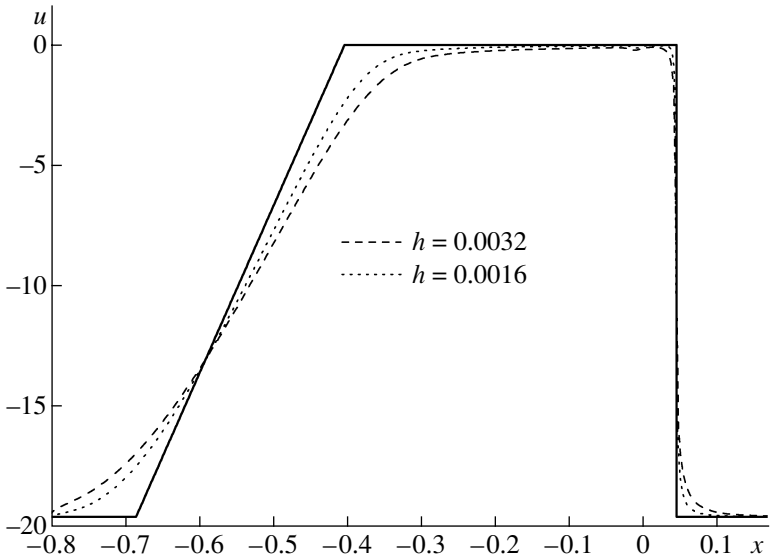

Fig. 14.

putational domain. In the entire flow region, except for the shock fronts, the velocity and the pressure gradient are identically zero: $u = 0$ and $dp/dx = 0$. Therefore, the regularizing additions proportional to τ vanish and the density and temperature perturbations are not smoothed. The only mechanism of smoothing the numerical perturbations is heat conduction. Therefore, a good numerical solution can be obtained by increasing the heat conduction (i.e., decreasing the Prandtl number). Figures 5–8 (fragments) display the solution as a function of the Prandtl number for Pr =1, 0.01, and 0.001. Figure 8 shows that an increase in the heat conduction has a negligible effect on the shape of the shock profile.

Figures 9 and 10 demonstrate that the density and velocity distributions at Pr = 0.001 converge rapidly as the mesh size is decreased. The temperature and pressure distributions also converge rapidly to the self-similar solution.

Thus, an increase in the artificial heat conduction in the QGD model leads to a fairly accurate solution of the Noh problem. Note that some of the algorithms discussed in [3, 4] lead to nonphysical oscillations, and the symmetry of the density profile is violated. In this example, as well as in the others, the QGD algo-

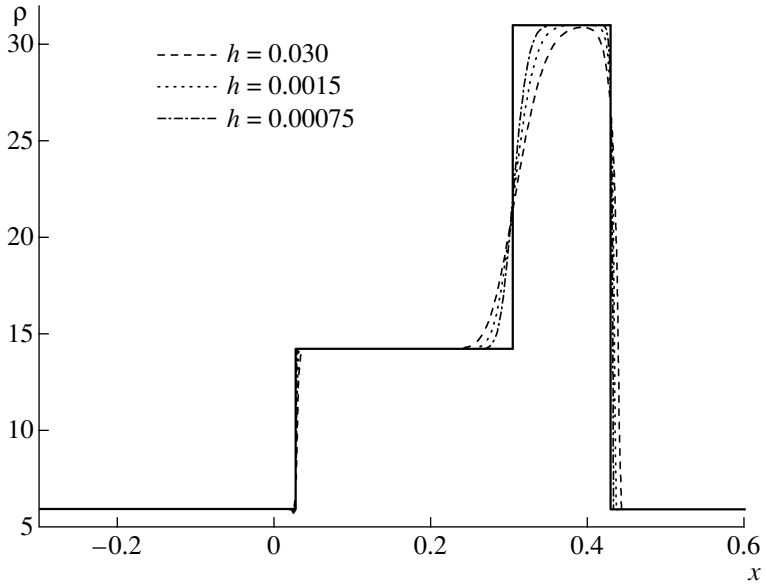

Fig. 15.

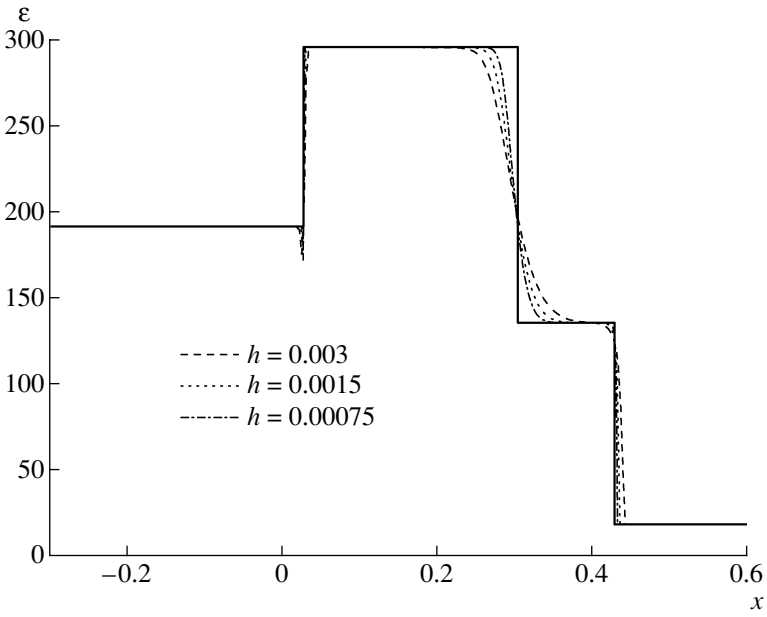

Fig. 16.

rithm produces an accurate numerical solution only on fairly fine grids. However, the computational costs associated with the degree of detail of the grid are balanced by the simplicity and computational efficiency of this algorithm.

Test 3a. This problem deals with the gas dynamic flow generated by gas compression in a thermonuclear target. The pressure drop p_L/p_R is 10^5, which corresponds to a temperature drop of the same order.

The regularization parameter for this problem was calculated at $\alpha = 0.7$. Smaller values of α led to an unstable solution at the contact discontinuity. The Courant number was $\beta = 0.01$ in all the computations. An increase in the artificial heat conduction (Pr = 0.1) led to a better numerical solution. Figure 11 shows the density as a function of the Prandtl number at $h = 0.0032$. The convergence of the numerical solution as the mesh size is decreased can be seen in Figs. 12–14. Specifically, Figs. 13 and 14 display fragments of the

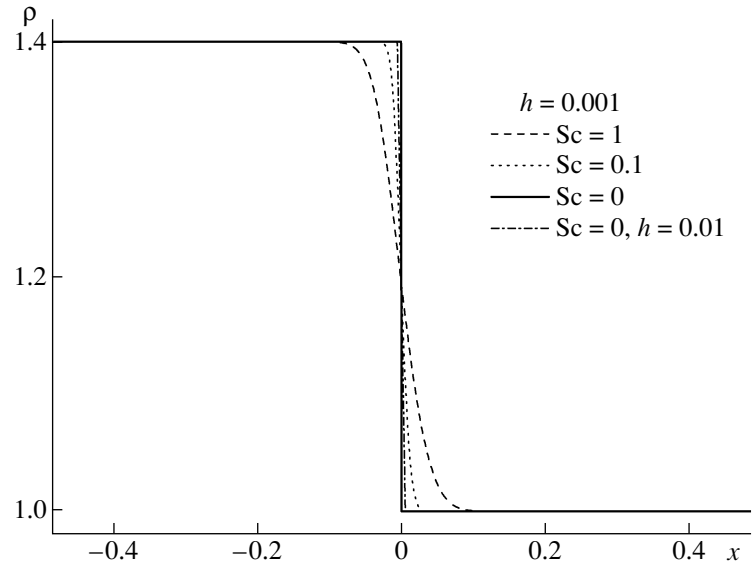

Fig. 17.

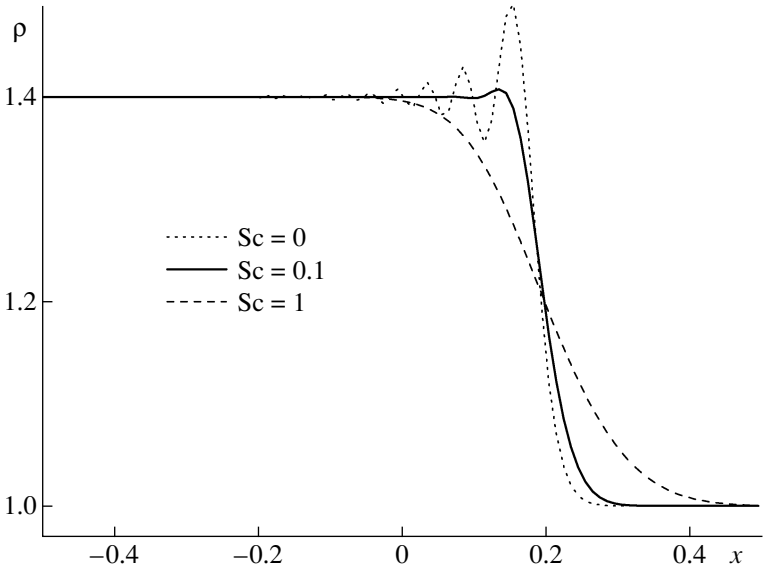

Fig. 18.

internal energy and velocity distributions. The front of a strong shock wave can be clearly seen at ~0.05. In these figures, the self-similar solution is shown by a solid line.

Test 4. This problem deals with a gas flow in the form of two diverging shock waves with a moving contact discontinuity in between. The ongoing processes proceed for short times. Therefore, the numerical solution to the problem is hardly dependent on the artificial heat conduction (Prandtl number).

The problem was solved with $\alpha = 0.4$ and $\beta = 0.1$. Figures 15 and 16 show the convergence of the numerical solution to the self-similar density and internal energy distributions (solid line) as the mesh size is decreased.

Test 5. The flow in this problem represents a stationary contact discontinuity. The problem was solved at $\alpha = 0.4$ and $\beta = 0.1$. Figure 17 demonstrates the effect of the viscosity and heat conduction on the numerical solution. It should be stressed that the viscosity and thermal conductivity are on the order of $\sim h$, and the corresponding terms are treated as numerical regularizers. The values of the viscosity and thermal conduc-

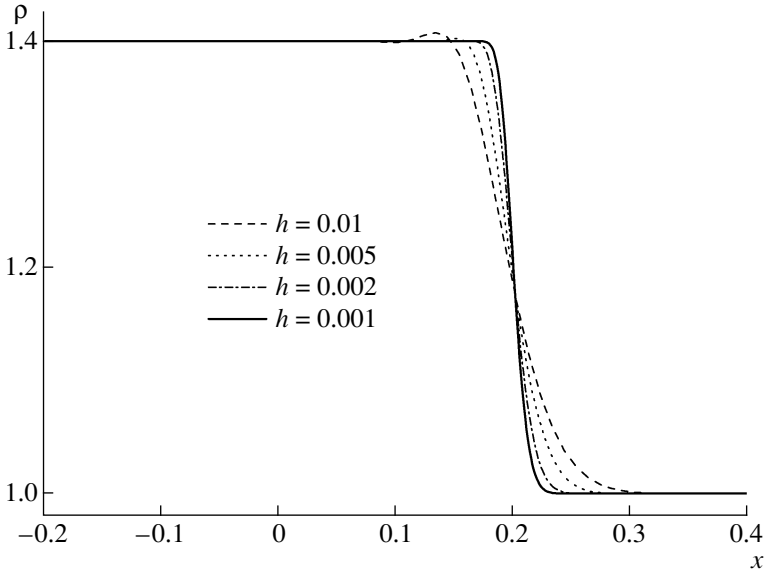

Fig. 19.

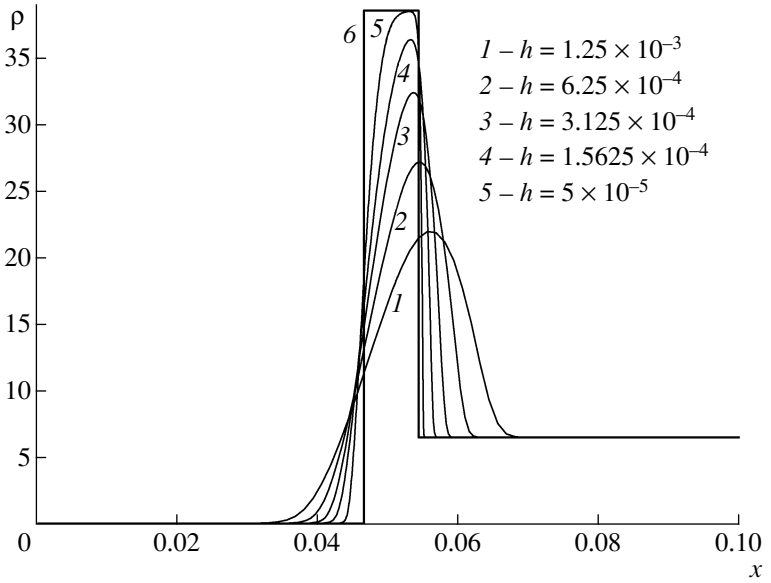

Fig. 20.

tivity are determined by Sc (see (9)). With the viscosity and heat conduction switched off (Sc = 0), the QGD algorithm as applied to this problem is accurate in the sense that the width of the contact discontinuity comprise one mesh spacing. This fact demonstrates the role of QGD dissipation, which stabilizes the stationary contact discontinuity, while the Navier–Stokes viscosity smears it. When the viscosity is switched off ($\tau = 0$), the solution is absolutely unstable.

Test 6. The problem deals with a slowly moving contact discontinuity. The computation was performed at $\alpha = 0.4$, $\beta = 0.1$, and Sc = 1. Figure 18 illustrates the effect of the viscosity and heat conduction at $h = 0.01$. It can be seen that a decrease in these coefficients (Sc = 0.1) leads to a more accurate numerical solution. However, when the Navier–Stokes artificial dissipation is totally switched off (Sc = 0), the solution exhibits oscillations. Figure 19 shows that the numerical solution at Sc = 0.1 converges as the mesh size is decreased.

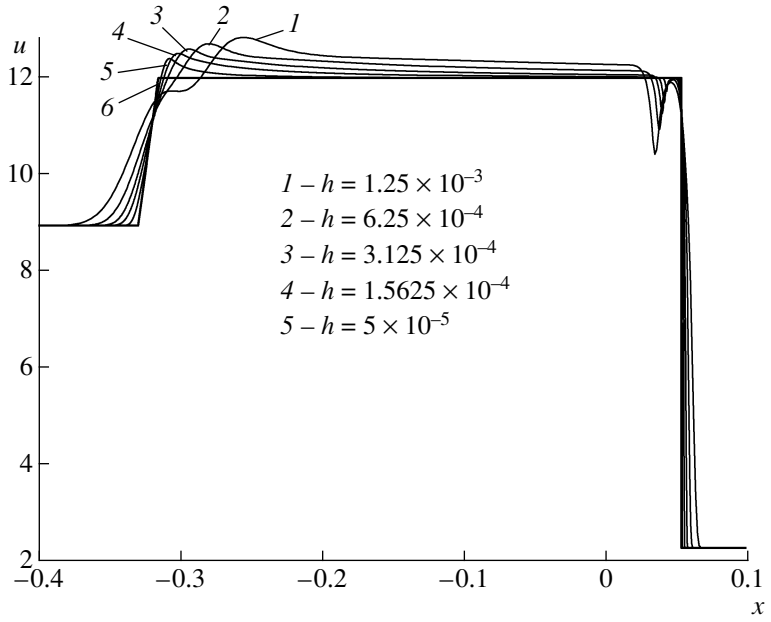

Fig. 21.

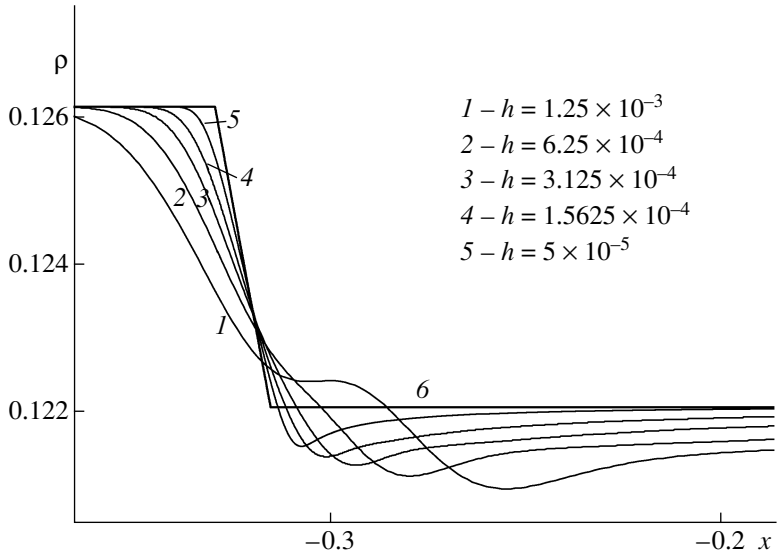

Fig. 22.

Test 7. The last test in the series of Riemann problems is the peak problem. This flow includes a strong shock wave with a density drop ~30, a rarefaction wave, and a contact discontinuity between them. The computation was performed at $\alpha = 0.3$, $\beta = 0.3$, $Sc = 1$, and $Pr = 1$. The numerical solution was smeared over the grid as α increased, while oscillations appeared at the fronts of the compression and rarefaction waves as α decreased. A decrease in the viscosity and thermal conductivity ($Sc = 0.1$) or only in the thermal conductivity ($Pr = 1000$) led to an unstable numerical solution.

For the density and velocity profiles, Figs. 20–22 show the convergence of the solution as the mesh size is decreased. As was noted in [3, 4], all the schemes discussed there have shortcomings concerning the computation of the velocity, especially in the neighborhood of a rarefaction wave ($x \sim -0.32$), where the density drop is very small and comprises ~0.004 (Fig. 22). In all the plots, the self-similar solution is depicted by line *6*.

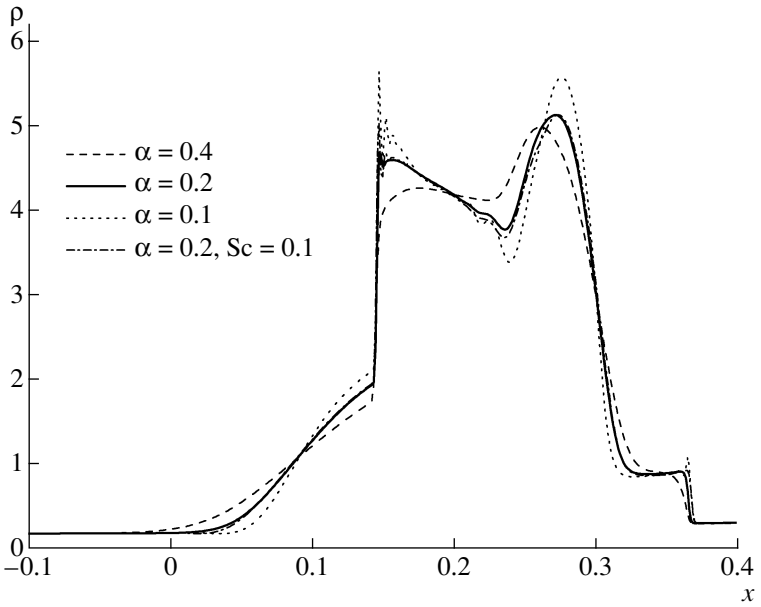

Fig. 23.

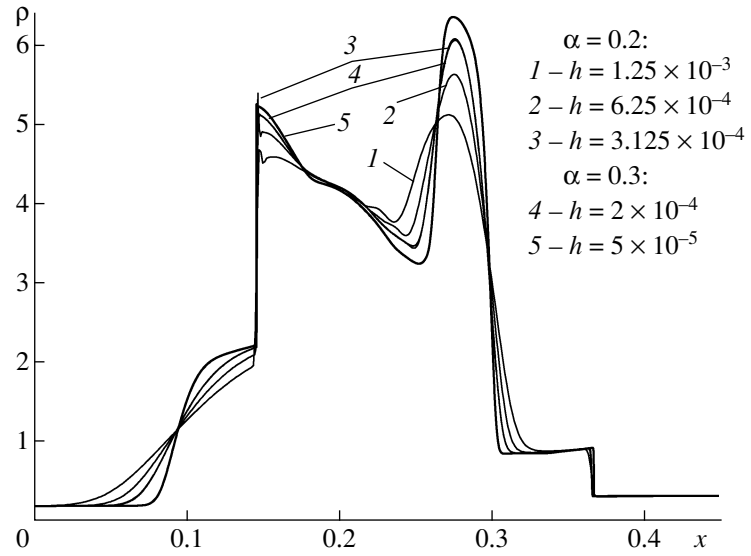

Fig. 24.

3. INTERACTION OF TWO SHOCKS

In this section, we solve the Woodward–Collela blast wave problem or the problem of interacting of two shocks (see [3, 4, 14]). In [15], this problem was used to test solution algorithms for the Euler equations on adaptive meshes.

The problem deals with the interaction of two waves generated by two Riemann discontinuities. It has no self-similar solution.

The problem was solved on the interval (–0.5, +0.5). Initially, discontinuities were specified at the points $x_1 = -0.4$ and $x_2 = 0.4$. In the entire computational domain, we set $\rho = 1$ and $u = 0$. The initial pressure values in the left (p_l), middle (p_m), and right (p_r) domains were specified as $(p_l, p_m, p_r) = (1000, 0.01, 100)$. Reflec-

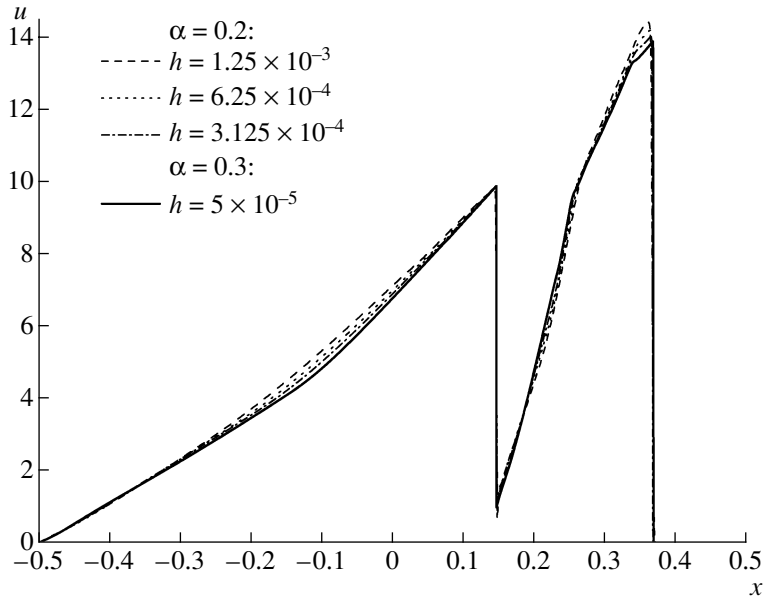

Fig. 25.

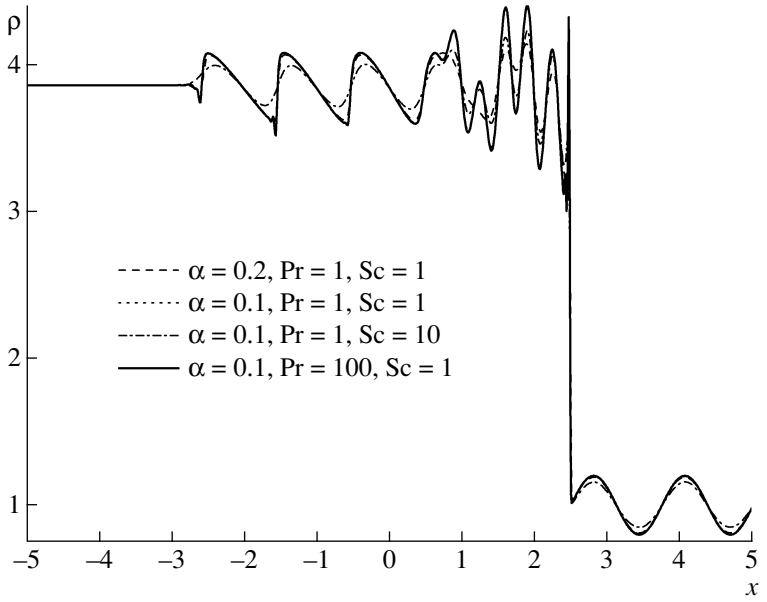

Fig. 26.

tion conditions of the form

$$\frac{\partial \rho}{\partial x} = 0, \quad \frac{\partial p}{\partial x} = 0, \quad u = 0$$

were set on the boundaries. The computations were conducted until the time $t_{\text{fin}} = 0.038$. We used $\gamma = 7/5$.

The optimal computational parameters are $\alpha = 0.3$, $\beta = 0.4$, Pr = 1, and Sc = 1. A decrease in α leads to oscillations in the density profile. A decrease in the viscosity and the thermal conductivity (Sc = 0.1) also leads to numerical instability (see Fig. 23). A decrease in the numerical thermal conductivity (Pr = 1000) has a negligible effect on the numerical solution, since the processes involved proceed on short time intervals.

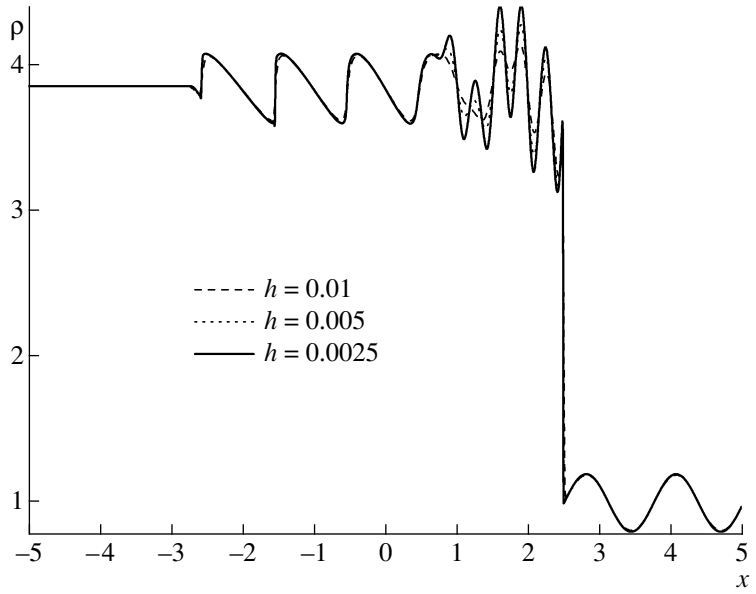

Fig. 27.

Figures 24 and 25 show the density and velocity distributions on a sequence of meshes for a regularization parameter with $\alpha = 0.3$ and 0.2. In this problem, the sensitive characteristics are the density, temperature, and internal energy distributions. The computations show that a fairly accurate density distribution is achieved only on fine meshes, while the velocity (Fig. 25) and pressure profiles are well resolved even on coarse meshes.

4. SHU–OSHER SHOCK ENTROPY WAVE INTERACTION PROBLEM

This problem was first suggested and numerically solved in [12]. The test shows the behavior of the difference algorithm in the case of the interaction of a smooth solution with a shock wave, namely, the interaction between a moving shock wave with a Mach number of 3 and a small entropy perturbation. As in the previous case, this problem has no self-similar solution.

This test is frequently used to test the capabilities of difference algorithms. For example, it was used in [13] to demonstrate the capabilities of high-order accurate difference schemes. In some works, this test was used to demonstrate the properties of schemes intended for computing turbulent flows in the framework of the LES approach (large eddy simulation). Below, the problem is considered in the statement described in [4].

The problem is solved in the domain (–5, 5). The discontinuity is at the point $x_0 = 4$. The initial conditions are similar to those in the Riemann problem: the values on the left interval are $(\rho_l, u_l, p_l) = (3.857143, 2.629369, 10.33333)$, while a smoothed density and constant velocity and pressure are specified on the right interval: $(\rho_r, u_r, p_r) = (1 + 0.2\sin(5x), 0, 1)$, $\gamma = 7/5$. The terminal computation time is $t_{\text{fin}} = 1.8$.

The optimal computational parameters are $\alpha = 0.2$, $\beta = 0.4$, $\text{Pr} = 1$, and $\text{Sc} = 1$. A decrease in α leads to oscillations in the density profile. An increase in α or the viscosity and thermal conductivity ($\text{Sc} = 10$) leads to an excessively smoothed solution. A decrease in the numerical thermal conductivity ($\text{Pr} = 100$) nearly does not affect the numerical solution (see Fig. 26, where $h = 0.01$). Figure 27 shows the convergence of the numerical solution at $\alpha = 0.2$ as the mesh size is decreased.

CONCLUSIONS

It was shown that the QGD method for computing the Euler equations can be used as a unified approach to the simulation of a wide class of unsteady gas dynamic flows. The numerical algorithm described includes two basic tuning parameters: the numerical coefficient α, which is involved in the regularization parameter τ, and the coefficient β, which determines the stability of the algorithm (the Courant number). In all the examples, α ranged from 0.2 to 0.5, while β ranged from 0.1 to 0.4. An exception was Tests 3 and

3a, which corresponded to superstrong shock waves and ultrahigh pressure drops with $\alpha = 0.5$ and 0.7 and $\beta = 0.001$ and 0.01, respectively.

In all the examples, the numerical solution converged to a reference solution as the spatial grid was refined.

For one-dimensional problems, the above study showed that the QGD algorithm produces solutions of the required quality on finer grids than in the methods studied in [3, 4, 9]. Nevertheless, the simple numerical implementation of the algorithm, its homogeneity, and the previously tested generalizations to multidimensional and unstructured meshes make the QGD approach competitive with other numerical methods intended for solving the Euler equations.

Due to the tuning parameters chosen for the QGD algorithm in the test examples with one-dimensional flows, multidimensional viscous flows and actual flows can be computed more effectively on unstructured grids, in which case the algorithm is difficult to tune.

REFERENCES

1. B. L. Rozhdestvenskii and N. N. Yanenko, *Systems of Quasilinear Equations* (Nauka, Moscow, 1978) [in Russian].
2. A. G. Kulikovskii, N. V. Pogorelov, and A. Yu. Semenov, *Mathematical Aspects of Numerical Solution of Hyperbolic Systems* (Fizmatlit, Moscow, 2001; Chapman and Hall/CRC, London, 2001).
3. R. Liska and B. Wendroff, *Comparison of Several Difference Schemes on 1D and 2D Test Problems for Euler Equations: Technical Report* (LA-UR-01-6225, LANL, Los Alamos, 2001).
4. R. Liska and B. Wendroff, "Comparison of Several Difference Schemes on 1D and 2D Test Problems for the Euler Equations," SIAM J. Sci. Comput. **25**, 995–1017 (2003).
5. Yu. V. Sheretov, *Mathematical Modeling of Fluid Flows Based on Quasi-Hydrodynamic and Quasi-Gasdynamic Equations* (Tversk. Gos. Univ., Tver, 2000) [in Russian].
6. T. G. Elizarova, M. E. Sokolova, and Yu. V. Sheretov, "Quasi-Gasdynamic Equations and Numerical Simulation of Viscous Gas Flows," Zh. Vychisl. Mat. Mat. Fiz. **45**, 544–555 (2005) [Comput. Math. Math. Phys. **45**, 524–534 (2005)].
7. T. G. Elizarova, *Quasi-Gasdynamic Equations and Methods for Computing Viscous Flows* (Nauchnyi Mir, Moscow, 2007) [in Russian].
8. B. N. Chetverushkin, *Kinetic Schemes and Quasi-Gasdynamic System of Equations* (Maks Press, Moscow, 2004) [in Russian].
9. E. Toro, *Riemann Solvers and Numerical Methods for Fluid Dynamics* (Springer-Verlag, Berlin, 1997).
10. I. A. Graur, "Splitting Finite-Difference Schemes for the Euler Equations Based on Quasi-Gasdynamic Equations," Zh. Vychisl. Mat. Mat. Fiz. **44**, 166–178 (2004) [Comput. Math. Math. Phys. **44**, 155–166 (2004)].
11. W. F. Noh, "Errors for Calculations of Strong Shocks Using An Artificial Viscosity and Artificial Heat Flux," J. Comput. Phys. **72**, 78–120 (1987).
12. C. Shu and S. Osher, "Efficient Implementation of Essentially Non-Oscillatory Shook-Capturing Schemes II," J. Comput. Phys. **83**, 32–78 (1989).
13. A. N. Kudryavtsev, T. V. Poplavskaya, and D. V. Khotyanovskii, "Application of Higher Order Accurate Schemes in Simulation of Unsteady Supersonic Flows," Mat. Model. **19** (7), 39–55 (2007).
14. P. Woodward and P. Colella, "The Numerical Simulation of Two-Dimensional Fluid Flow with Strong Shocks," J. Comput. Phys. **54**, 115–173 (1984).
15. P. V. Breslavskii and V. I. Mazhukin, "Modeling of Shock Interaction on Dynamic Adaptive Meshes," Mat. Model. **19** (11), 83–95 (2007).